To the Graduate Council:

I am submitting herewith a thesis written by Timothy Bain Ervin entitled “A Finite Element Evaluation of Talocrural Joint and the Effects of Ligament Injury on Joint Mechanics.” I have examined the final electronic copy of this thesis for form and content and recommend that it be accepted in partial fulfillment of the requirements for the degree of Master of Science, with a major in Engineering.

Ronald U. Goulet
Associate Professor

We have read this thesis and
recommend its acceptance:

Joseph O. Owino

Gary B. Wilkerson

Richard G. Alvarez

Accepted for the Council

Stephanie L. Bellar
Interim Dean of the
Graduate School

A FINITE ELEMENT EVALUATION OF THE TALOCRURAL JOINT AND THE EFFECTS OF LIGAMENT INJURY ON JOINT MECHANICS

A Thesis

Presented for the

Master of Science

Degree

The University of Tennessee, Chattanooga

Timothy Bain Ervin

May 2010

Dedication

This thesis is dedicated to my wife and two daughters Amy Ervin, River Ervin, and Bailey Ervin, for their patience and support, and my parents, George Ervin and Kathy Ervin.

Acknowledgements

I would like to acknowledge the help and support given to me by Dr. Ron Goulet throughout my graduate experience and during my thesis process. He has always been there to help me when I had questions or needed direction. I would also like to thank Jim Harrison of WJH Engineering for providing access to his license of ABAQUS and Hypermesh and for all the support and help he gave me in troubleshooting my finite element model. I would like to think Dr. Gary Wilkerson for his guidance in the area of ankle injury and instability and for taking the time to explain the mechanics of ankle injury and to demonstrate advances with in vivo measurement devices. I would like to think Dr. Joseph Owino for teaching me the fundamentals of finite element analysis and providing me the background needed to pursue this undertaking. I would like to think Dr. Richard Alvarez for explaining to me the anatomy of the ankle and for answering questions regarding the field of orthopaedics and treatment of foot and ankle pathologies. I would like to thank Dr. Jesse Doty for his help during the in vitro testing; his suggestions and surgical skill resulted in a successful test. I would like to thank all the members of my thesis committee for their time and support.

Abstract

Several cadaveric and in vivo biomechanical studies have looked at the effects that ligament injuries of the ankle joint complex have on the stability of the ankle joint and susceptibility to chronic degeneration of articular surfaces, but there have been very few studies that use computer simulation and the finite element method to evaluate how an ankle ligament injury affects stability, joint pressure, and potential subsequent failure points. Evidence shows that ankle instability is associated with excessive rotation of the talus in transverse plane, which contributes to articular surface degeneration. It has been documented that after disruption of the anterior talofibular ligament that additional load is placed on the posterior tibiotalar ligament, which leads to further rotational instability. Disruption of the interosseous talocalcaneal ligament creates a more complex instability that leads to chronic joint instability of both the talocrural and subtalar joints. A 3D model of the ankle joint was created using CT image data of a cadaver lower limb. A tetrahedral mesh was created and the bone modulus was assumed uniform. Tendons were represented by simple truss elements and surface to surface contact regions were established to facilitate joint motion. The tibia was fixed and internal rotation in the transverse plane was applied to the foot in the neutral position by means of a 5000 N-mm moment. Force displacement data was compared to experimental data collected using an MTS test frame on a cadaver specimen, and previously published data from an arthrometer study. The anterior talofibular ligament (ATFL) was then removed and compared to MTS and arthrometer load and displacement data. Joint pressures were calculated from the finite element model to evaluate potential lesion spots as well as ligament forces in the deep posterior tibiotalar ligament (DPTTL). Results show a correlation in the change in magnitude from intact to ATFL cut states in the FEA model to the in vitro testing methods. The model predicts a medial shift in contact pressures under internal rotation which has been shown to be a potential location for lesions in ankles with lateral instability. The model also predicts that the DPTTL carries a majority of the resistant forces in the ligaments in internal rotation when the ATFL has been compromised.

Preface

The field of orthopaedics is relatively new compared to other more established fields of medicine. Biomechanical research through in vitro and in vivo studies has only flourished in the last 100 years, with major advances coming in the last half of that period. It was only during the Vietnam War that the standard of care for war injuries was changed from amputation to limb salvage. During the space race of the 1960's, NASA designed and built the first cohesive finite element analysis package NASTRAN. This opened the door to finite element analysis in other fields of engineering; during the 1980's it was in the early stages of being used in orthopaedics. Today finite element analysis is heavily used in all aspects of orthopaedics and is used extensively by industry for the design and development of new orthopaedic products. Because of its prevalence there has been significant research to develop better models to represent the complex mechanical properties of biological tissues, with major advances in non-linear contact models as well as anisotropic, viscoelastic, and hyperelastic material behavior models.

Table of Contents

List of Tables

List of Figures

Nomenclature

kN	kilonewton
mm	millimeter
mm/s	millimeters per second
mm^2	square millimeter
mm^3	cubic millimeter
MPa	mega pascal
N	newton
N-m	newton meter
N-mm	newton millimeter
s	second
tonne	metric ton
$tonne/mm^3$	metric ton per cubic millimeter

Abbreviations

ATFL	Anterior Talofibular Ligament
CAD	Computer Aided Design
CFL	Calcaneofibular Ligament
CT	Computed Tomography
DATTL	Deep Anterior Tibiotalar Ligament
DICOM	Digital Imaging and Communications in Medicine
DPTTL	Deep Posterior Tibiotalar Ligament
E	Modulus of Elasticity
FEA	Finite Element Analysis
MRI	Magnetic Resonance Imaging
PTFL	Posterior Talofibular Ligament
STL	Stereo Lithography File
TCL	Tibiocalcaneal Ligament
TNL	Tibionavicular Ligament

Chapter 1 Introduction

1.1 Background

Several cadaveric and in vivo biomechanical studies have looked at the effects that ligament injuries of the ankle joint complex have on the stability of the ankle joint and susceptibility to chronic degeneration of articular surfaces (McCullough and Burge 1980, Rasmussen and Kromann-Andersen, Experimental Ankle Injuries 1983, Renstrom, et al. 1988, Birmingham, et al. 1997, Conlin, Johnson and Sinning 1989, Dias 1979, Xenos, et al. 1995, Teramoto, et al. 2008), but there have been very few studies that use computer simulation and the finite element method to evaluate how an ankle ligament injury affects stability, joint pressure, and potential subsequent failure points. (Cheung and Zhang 2006, Iaquinto and Wayne 2008, Anderson, et al. 2006) Evidence shows that ankle instability is associated with excessive rotation of the talus in transverse plane, which contributes to articular surface degeneration. (Rasmussen and Tovborg-Jensen, Anterolateral Rotational Instability in the Ankle Joint 1981, Johnson and Markolf 1983) It has been documented that after disruption of the anterior talofibular ligament that additional load is placed on the posterior tibiotalar ligament, which leads to further rotational instability. (Stormont, et al. 1985) Disruption of the interosseous talocalcaneal ligament creates a more complex instability that leads to chronic joint instability of both the talocrural and subtalar joints. (Wilkerson, et al. 2005, Parlasca, Shoji and D'Ambrosia 1979, Wilkerson and Alvarez, Rotary ankle instability: Pathomechanics and consequences of inadequate treatment. 2010 (in press)) Resent research (Wilkerson, Doty, et al. 2010 (in press)) has shown the effectiveness of using an ankle arthrometer to record the transverse plane rotation and torque curve of an ankle then comparing the curve to the curve of a normal ankle. A normal ankle curve exhibits some elastic hysteresis, but ligament injuries to the ankle increase rotary displacement creating backlash in the force displacement curve. The presence and severity of an injury can be evaluated as well as subsequent repair. (Johnson and Markolf 1983, Wilkerson, Doty, et al. 2010 (in press))

1.2 Objective

The objective of this thesis was to develop a finite element model of the talocrural joint in an intact state and in an ATFL removed state. The load displacement results of the finite element model would then be validated by in vitro testing and contact pressure patterns would be compared to clinical data of ankle lesions in laterally unstable ankles.

Chapter 2 Ankle Joint Properties

2.1 Bone Mechanical Properties

Human bone is comprised of two distinct subtypes of bone cortical and cancellous. Cortical bone is harder and stiffer than cancellous bone due to cellular size and density, but recent studies show that cortical bone is stronger than previously thought. Both types of bone exhibit anisotropic behavior which means more parameters, such as elastic modulus, Poisson's ratio, and shear modulus for all three loading directions are needed to properly specify behavior of these materials. Strain rate must also be known since bone is also viscoelastic. Because of the anisotropic and viscoelastic behavior, bone is classified as a complex material. In long bones it can be assumed that cortical bone will behave as a transversely isotropic material meaning that it is isotropic about its axis and exhibits a secondary isotropic modulus in the transverse plane.

2.2 Ligament Mechanical Properties

Ligaments are comprised of parallel collagen fibers and are therefore best represented by transverse isotropic material behavior. They exhibit a non-linear concave upward load elongation curve during initial loading changing to a linear elastic region as strain increases. The cause of the change in stiffness is due to an initial un-crimping of the collagen fibers, once the fibers un-crimp the collagen fiber backbone is then being stretched resulting in a higher stiffness. Most of the physical loading conditions are done in the non-linear region, occasionally in the linear region Ligaments have also been shown to exhibit the viscoelastic characteristics of creep, stress relaxation, and hysteresis. Ligaments have even been shown to exhibit hyperelastic properties by exhibiting elastic behavior even under very high strain. (Mow and Huiskes 2005)

2.3 Articular Cartilage Mechanical Properties

Articular cartilage is a biphasic material due to water flowing through the porous permeable solid matrix of cartilage under an imposed pressure gradient during loading. Its mechanical properties are very similar to a sponge which has a high resistance to fluid flow. (Mansour 2004, Mow and Huiskes 2005) Cartilage can exhibit both isotropic and anisotropic behavior as well as viscoelastic and hyperelastic behavior based on location in the body, loading direction, strain rate, and hydration. The main mechanism for the viscoelastic properties of articular cartilage are the hydroscopic drag as fluid moves through the membranes of the cartilage structure. The hyperelastic properties of articular cartilage are due to its incompressibility and

ability to undergo large amounts of strain without permanent deformational while still remaining in the elastic region of its stress strain curve.

2.4 Ankle Joint Biomechanics

The ankle joint complex consist of a series of joints each contributing to the overall range of motion of the ankle. The first component is the ankle joint or talocrural joint formed by the tibia, fibula, and talus. This joint is followed by the sub-talar joint formed by the talus and calcaneus. The last joint is the transverse tarsal joint which consists of the talonavicular and calcaneocuboid joints formed by the talus, navicular, cuboid, and calcaneus bones. (Mann and Haskell 2007, Netter 2003) The range of motion starting in the neutral position for a normal ankle joint complex is 33º to 18º in inversion-eversion and 48º to 18º plantarflexion-dorsiflection. (American Academy of Orthopaedic Surgeons 1965) The talocrural joint is stabilized by a set of ligaments consisting of the ATFL, CFL, PTFL, DPTTL, TCL, DATTL, and TNL. While most internal rotation of the foot comes from the hip joint during normal walking some internal rotation comes from the ankle joint. An increase in internal rotation is usually associated with lateral ankle instability from a ligament injury. (Dias 1979)

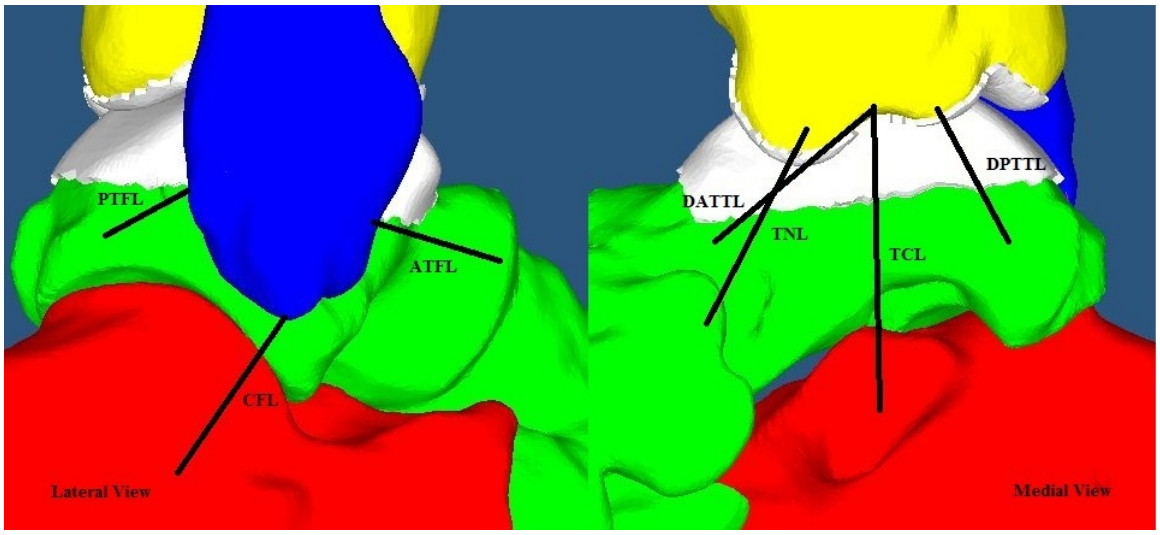

Figure 1 Ankle Joint Ligaments

The ligaments of the ankle are shown in the lateral and medial views. The ATFL, CFL, PTFL, DATTL, TNL, TCL, and DPTTL are visible.

Chapter 3 Methods

3.1 Overview

A 3D model of the ankle joint was created using CT image data of a cadaver lower limb. A tetrahedral mesh was created and the bone modulus was assumed uniform. Tendons were represented by simple truss elements and surface to surface contact regions were established to facilitate joint motion. The tibia was fixed and internal rotation in the transverse plane was applied to the foot in the neutral position by means of a 5000 N-mm moment. Force displacement data was compared to experimental data collected using an MTS test frame on a cadaver specimen, and previously published data from an arthrometer study (Wilkerson, Doty, et al. 2010 (in press)). The anterior talofibular ligament (ATFL) was then removed and compared to MTS and arthrometer load and displacement data. Joint pressures were calculated from the finite element model to evaluate potential lesion spots as well as ligament forces in the posterior tibiotalar ligament (PTTL).

Figure 2 MTS 858 Mini Bionix II

The MTS 858 Mini Bionix is a biaxial test frame capable of testing both axial and torsional loading conditions simultaneously. The testing fixture was custom built to accommodate the finite element model boundary conditions. The fixture consisted of a set of linear bearings and a gimbaled fixture. This setup allowed for medial-lateral translation, proximal-distal translation, internal-external rotation, and varus-valgus tilt.

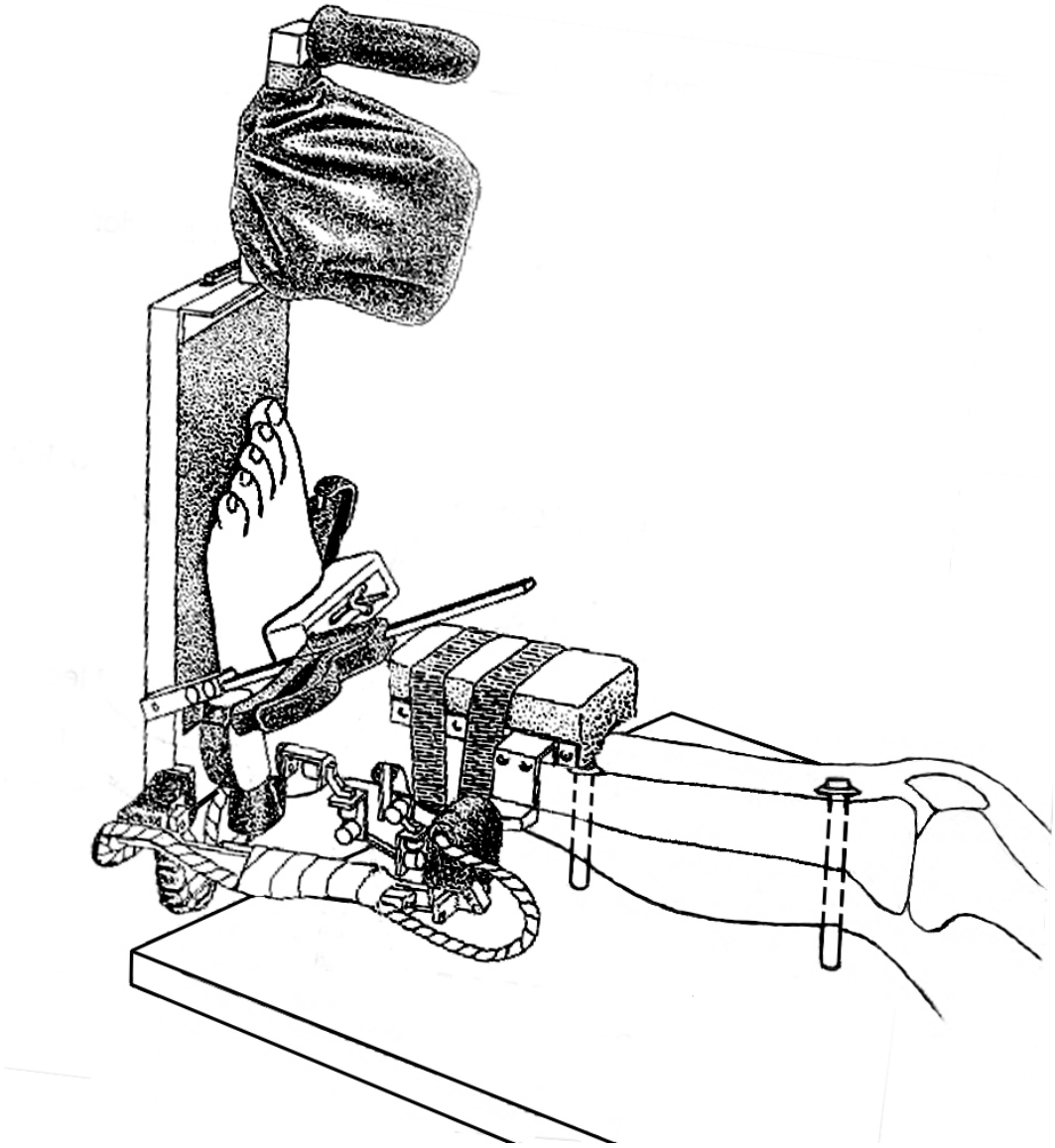

Figure 3 Ankle Arthrometer

The ankle arthrometer was developed by Blue Bay Research (Navarre, FL) for diagnosing ankle ligament injuries in vivo. It can also be used in vitro to assess the function of the ankle before and after removal of ligaments, and to assess the effects of repair and various taping methods. The arthrometer shown in the above figure is the original model which is capable of only measuring the translations and reaction loads of the ankle joint complex. The current arthrometer and the one used for the study is able the measure translations and reaction loads as well as measure rotations and reaction torques of the ankle joint complex.

3.2 Finite Element Model Development

3.2.1 Meshing

CT imaging results in a series of sequential dicom image slices through the foot and ankle taken at a resolution of 16 slices per inch. These dicoms were imported into Slicer3D (3D Slicer home page 2010, Pieper, Halle and Kikinis, 3D SLICER 2004, Pieper, Lorensen, et al. 2006, Gering, et al. 1999) and threshold values were set that corresponded to the grey scale density of cortical bone. Slicer3D then interpolated the dicom images to create a rendered volume of the foot and ankle comprised of a dense collection of polygon volumes. Slicer3D then converted the resulting volume into a stereo lithography file (.stl) that was comprised of a dense mesh of triangle surfaces. The stl file was then imported into Hypermesh (Altair, Troy, MI) for preprocessing. Once the file was imported to Hypermesh a wrap was done of the stl surfaces to create a hollow shell of 2D triangle elements. A tetrahedral mesh was then created to fill in the hollow 2D Mesh. Articular cartilage was extruded with 6-node prism elements to a thickness of 1 mm. (El-Khoury, et al. 2004, Shepherd and Seedhorn 1999) Special tension only truss elements were used to define the ligaments of the ankle and were connected to nodes at the point of anatomical insertion. (Cheung and Zhang 2006)

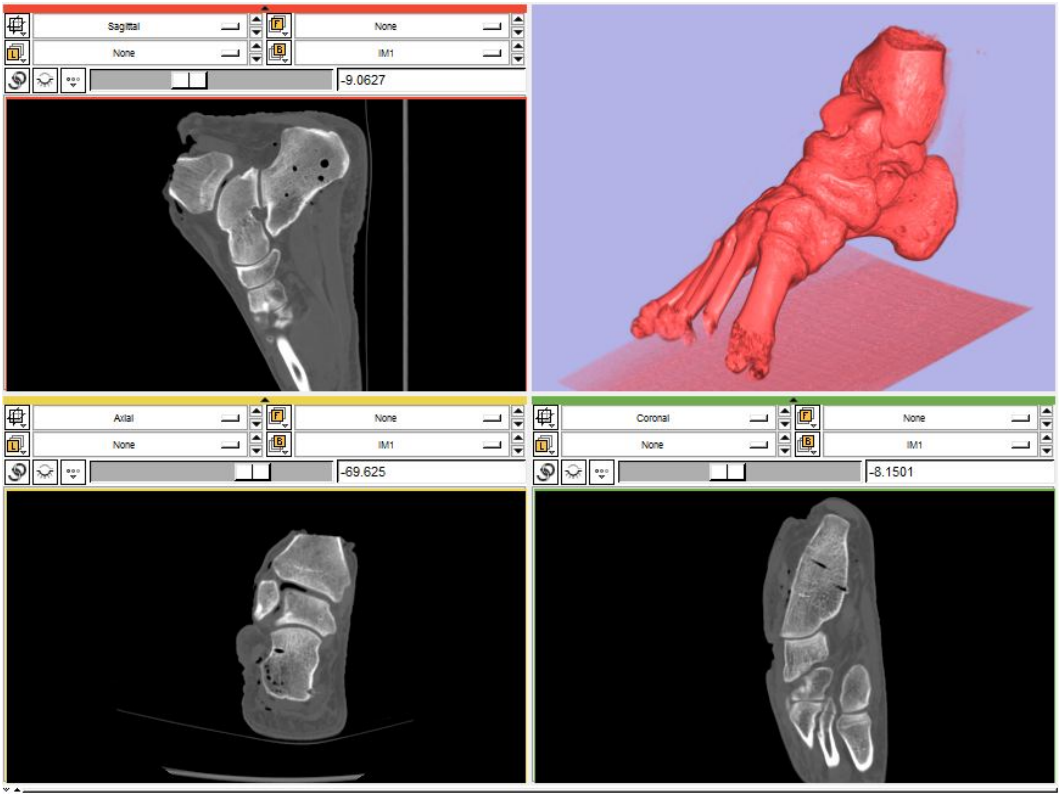

Figure 4 Dicom Images and Volume Rendering

Silcer3D (3D Slicer home page 2010) is open source software that is capable of assembling dicom sets from either CT or MRI imaging then converting them into a 3D model. Once a 3D model of polygon elements has been created in Slicer3D it can be converted into a STL file consisting of triangle elements. The STL file is a commonly accepted file format in most meshing and 3D CAD program import functions.

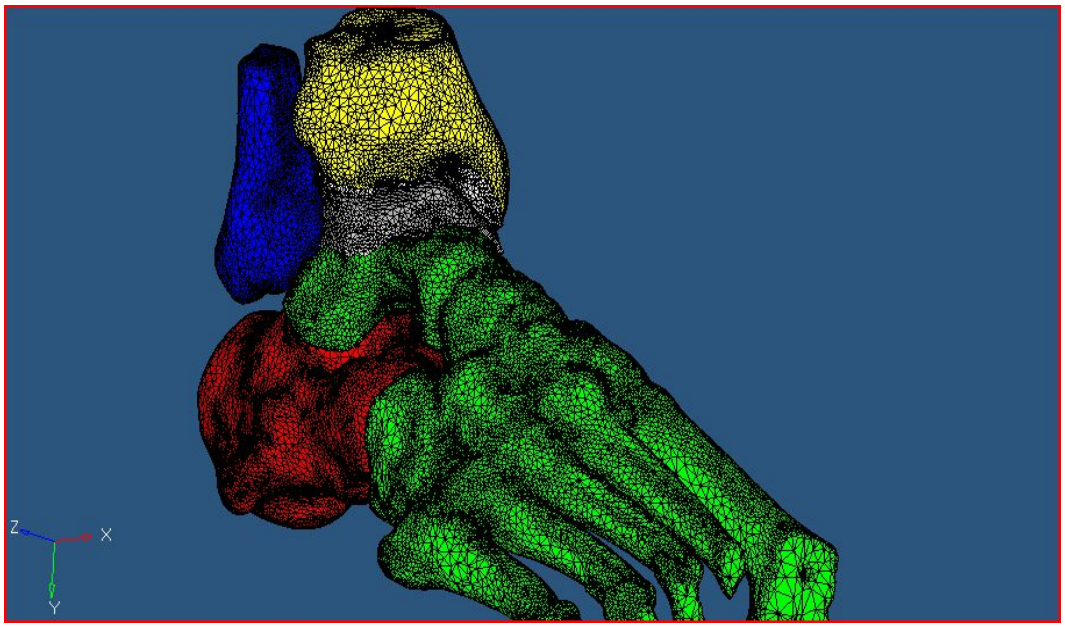

Figure 5 Meshed Model

The finite element model consists of a 3D tetrahedral mesh of the tibia, fibula, talus, calcaneus, and forefoot. Articular cartilage structures were extruded on both the talar dome and the distal tibia with 6-node prism elements. Tension only 2-node truss elements were placed in the anatomic locations for the ATFL, CFL, PTFL, DPTTL, DATTL, TCL, and TNL. All elements were modeled as linear elastic materials.

3.2.2 Model Parameters

The modulus of the bone was assumed uniform, elastic, and isotropic since the main focus is that of joint motion and not for the stresses in the bone itself. A value of 16000 MPa was used for the bone's modulus and a Poisson's ratio of 0.3 was used. (Mow and Huiskes 2005) Cartilage was also assumed to be elastic and isotropic. A value of 10 MPa was used for the modulus and a Poisson's ratio of 0.3 was used. (Mansour 2004) Ligaments were given a tension only elastic modulus of 158 MPa and a Poisson's ratio of 0.3 were used. (Attarian, et al. 1985, Colville, et al. 1990, Siegler, Brock and Schneck 1988, St. Pierre, et al. 1983) The cross section of each ligament was defined from values available in literature. (Mkandawire, et al. 2005) Density was assigned for the bone, cartilage, and ligaments at values of 1.5e-9, 1.0e-9, and 1.0e-9 tonne/mm^3 respectively. Contact between the articular cartilage surfaces was modeled as "soft" or exponential contact. Values were assigned for the distance at which contact first engages and the value for the force exerted. The distance value was 0.0001 mm and the force value was 0.01 N. Friction was modeled as classic Coulomb friction with a value of 0.001 and a maximum shear stress value of 1 Pa. The very small 1 Pa force was assigned arbitrarily to facilitate a faster convergence of the finite element model, since zero was mathematically less stable. The maximum shear stress value is the value at which sliding will occur regardless of normal contact stress. (Abaqus 2007) During the internal rotation phase the value of the friction and max shear stress were set to zero, the reason is that articular cartilage surface friction can be assumed zero in the presence of synovial fluid. (Mansour 2004)

Table 1 FEA Model Material Properties

Material Type	Modulus (MPa)	Poisson's Ratio	Density (tonne/mm^3)
Bone	16000	0.3	1.5e-9
Articular Cartilage	10	0.3	1.0e-9
Ligaments	158	0.3	1.0e-9

Table 2 FEA Model Ligament Cross-Sections

Ligament Abbreviation	Cross-Section Area (mm^2)
ATFL	62.85
CFL	21.36
DPTTL	78.43
DATTL	43.49
PTFL	46.43
TCL	43.2
TNL	60

3.2.3 Boundary Conditions and Loading Methods

Even though it has been stated that anterior translation contributes to instability in the ankle by allowing the talus to rotate out of the mortis of the ankle joint, anterior-posterior translation was fixed. The reason for this was that the model was limited to bones, cartilage, and ligaments. Without the joint capsule and surrounding soft tissue the ankle joint will completely disarticulate in the absence of the ATFL, and is numerically unstable in a finite element analysis. Medial-lateral translation was set to free as well as proximal-distal translation, varus-valgus tilt, and internal-external rotation. Plantarflexion-dorsiflection rotation was fixed to hold the foot in the neutral plane during internal rotation. A static load of 100 N was applied in the proximal direction through the talus to seat the ankle, and then a torque of 5000 N-mm was applied to induce internal rotation of the ankle. The torque was removed and the ankle was allowed to return to its initial state. The ATFL was removed and the cycle was repeated.

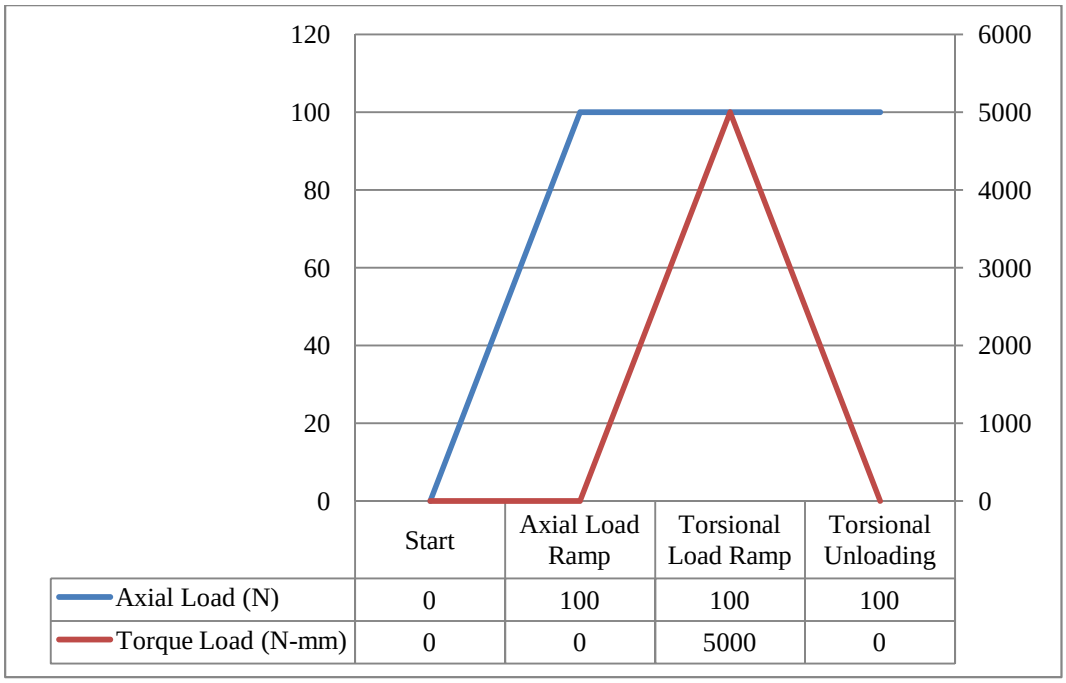

Figure 6 Loading Profiles

The loading profile of the in vitro and FEA test consists of an axial load of 100 N that is applied at the beginning and is held through the test duration. The torque load of 5000 N-mm (5 N-m) is applied and then released. This test cycle is done for both the intact state and ATFL cut state.

3.2.4 Finite Element Analysis

The finite element analysis model was calculated in the ABAQUS multi physics software package (Simulia, Providence, RI). special consideration was taken for the discontinuous nature of the ankle model. ABAQUS stabilization features were used during the initial loading phase and to a lesser degree during the internal rotation phase with the ATFL removed. The stabilization feature places an energy cushion in the void around the contact surfaces and decreases that energy to zero by completion of the step. The auto tolerance function was used to calculate the over-closure tolerances for contact to assist in the initial contact phase. The model was treated as a discontinuous analysis. This allows ABAQUS to use more equilibrium iterations and prevents the analysis time step from being decrease early in the analysis. (Abaqus 2007) During the axial loading step the analysis was treated as dynamic instead of static as in the rest of the analysis; this was due to large amounts of ridge body motion combined with two contact surfaces coming into full contact. After this step the remainder or the analysis was semi-static.

3.2.5 Post Processing

Post processing was done in ABAQUS CAE. Tables of X-Y data were created for the proximal and distal sections of the ankle, giving load and rotation verses time. Contact profiles were also created for comparison to known cartilage lesion locations in unstable ankles.

3.3 In Vitro Biomechanical Test Validation

3.3.1 Specimen Preparation

The original fresh frozen specimen that was used to create 3D model could not be used for testing due to damage to the CFL and ATFL, so a different fresh frozen specimen that was similar in size and age was used. The specimen was thawed from -20º C to room temperature and then placed in a custom fixture purpose built to replicate the boundary and loading conditions of the finite element model. Linear bearings allow for free movement in the medial-lateral direction as well as free varus-valgus tilt. Anterior-posterior movement was restricted as well as plantarflexion-dorsiflection rotation. A single 4.5 cancellous lag screw was placed through the calcaneus and through the subtalar joint into the talar dome to prevent subtalar joint motion. The foot was secured by two traction pins one through the calcaneus and one through the navicular and cuboid bones. Both pins were secured to the testing jig by means of external fixator locknuts. The tibia and fibula were potted in a steel cylinder by means of a quickset epoxy.

Figure 7 In Vitro Test Setup

The in vitro test setup was performed on a fresh frozen ankle specimen. The specimen was thawed and then soft tissue resected to allow for the potting of the fibula and tibia in a steel cylinder with epoxy. A single 4.5mm cancellous lag screw was used to secure the sub talar joint and the calcaneus, navicular, and cuboid bones were fixed using two traction pins.

3.3.2 Testing Protocol

Axial force and internal rotation torque were applied by a MTS 858 Mini Bionix test frame (MTS, Eden Prairie, MN). Loading rates were 10 N per second for axial force and 100 N-mm per second for internal rotation. Data acquisition rates were 40Hz for all recorded measurements. Load data was acquired from the MTS frame 15 kN biaxial load cell and rotation and axial displacement will be recorded by the MTS rotary and linear variable displacement transducers respectively. Axial displacement was measured in mm and internal rotation was measured in degrees. First an axial load of 100 N was applied to seat the joint and then it was followed by an internal rotation torque of 5000 N-mm. After full torsional loading the torque load was returned to 0 N-mm and the ankle was allowed to return to its new resting position. The specimen was unloaded and the ATFL cut at its mid-length. The loading cycle was repeated for the ankle now with a cut ATFL.

3.3.3 Post processing of Raw Data

Load and displacement data was exported to Excel and was formatted into Torque vs. Internal Rotation graphs. Raw data was smoothed by averaging every 100 data points; the smoothed data was then interpolated at 5 distinct positions 1, 2, 3, 4, and 5 N-m for comparison to other measurement methods.

Chapter 4 Results

The results of the FEA model show a decreased amount of displacement compared to the two in vitro testing methods. At max internal rotation there is an 88% difference in the intact state and a 51% difference in the ATFL removed state between the FEA model and in vitro testing on the MTS. There is also a 90% difference in the intact state and a 48% difference in the ATFL removed state between the FEA model and in vitro testing on the arthrometer. A comparison of max internal rotation of the two in vitro testing methods shows a 15% difference in the intact state and a -7% difference in the ATFL removed state between the MTS and the arthrometer. The correlation in the change in magnitude between the intact state and ATFL state calculated by the FEA model and the in vitro methods was 86% of the FEA model prediction for the MTS and 44% for the arthrometer.

The ligament forces calculated by the FEA model at max internal rotation in the intact state show a force of 179 N in the ATFL and forces of approximately 0 N in the other ligaments. In the ATFL removed state the FEA model shows a force of 7 N in the CFL and 156 N in the DPTTL the forces in the other remaining ligaments are approximately 0 N.

Contact pressures calculated by the FEA model show a contact profile that is laterally biased ranging from 0 to 2.5 MPa for the intact and ATFL removed states at 0 N-m of applied internal rotation moment. In the intact state at 5 N-m of applied internal rotation moment the contact profile becomes more distributed with a 2 MPa maximum. The ATFL removed state at 5 N-m shows a posterior medial shift in contact as well as anterior contact between the lateral side of the talar dome and the tibial malleolus with an increased pressure range o f 3.8 MPa.

Table 3 Comparison of FEA Model Data and In Vitro Testing Data

	Internal Rotation (Degrees)					
	FEA Model		In Vitro		% Difference	
Moment (N-m)	Intact	-ATFL	Intact	-ATFL	Intact	-ATFL
1.0	0.37	1.47	1.76	2.66	78.98	44.74
2.0	0.73	5.85	8.05	8.74	90.93	33.07
3.0	1.08	9.88	11.46	13.68	90.58	27.78
4.0	1.43	10.92	13.36	16.79	89.3	34.96
5.0	1.77	11.44	15.06	23.44	88.25	51.19

Table 4 Comparison of FEA Model Data and Arthrometer Data

	Internal Rotation (Degrees)					
	FEA Model		Arthrometer		% Difference	
Moment (N-m)	Intact	-ATFL	Intact	-ATFL	Intact	-ATFL
1.0	0.37	1.47	6.70	7.09	94.48	79.27
2.0	0.73	5.85	11.22	12.70	93.49	53.94
3.0	1.08	9.88	14.14	16.96	92.36	41.75
4.0	1.43	10.92	16.08	18.98	91.11	42.47
5.0	1.77	11.44	17.62	21.89	89.95	47.74

Table 5 Comparison of In Vitro Testing Data and Arthrometer Data

	Internal Rotation (Degrees)					
	In Vitro		Arthrometer		% Difference	
Moment (N-m)	Intact	-ATFL	Intact	-ATFL	Intact	-ATFL
1.0	1.76	2.66	6.70	7.09	73.73	62.48
2.0	8.05	8.74	11.22	12.70	28.26	31.18
3.0	11.46	13.68	14.14	16.96	41.37	19.34
4.0	13.36	16.79	16.08	18.98	16.92	11.54
5.0	15.06	23.44	17.62	21.89	14.53	-7.44

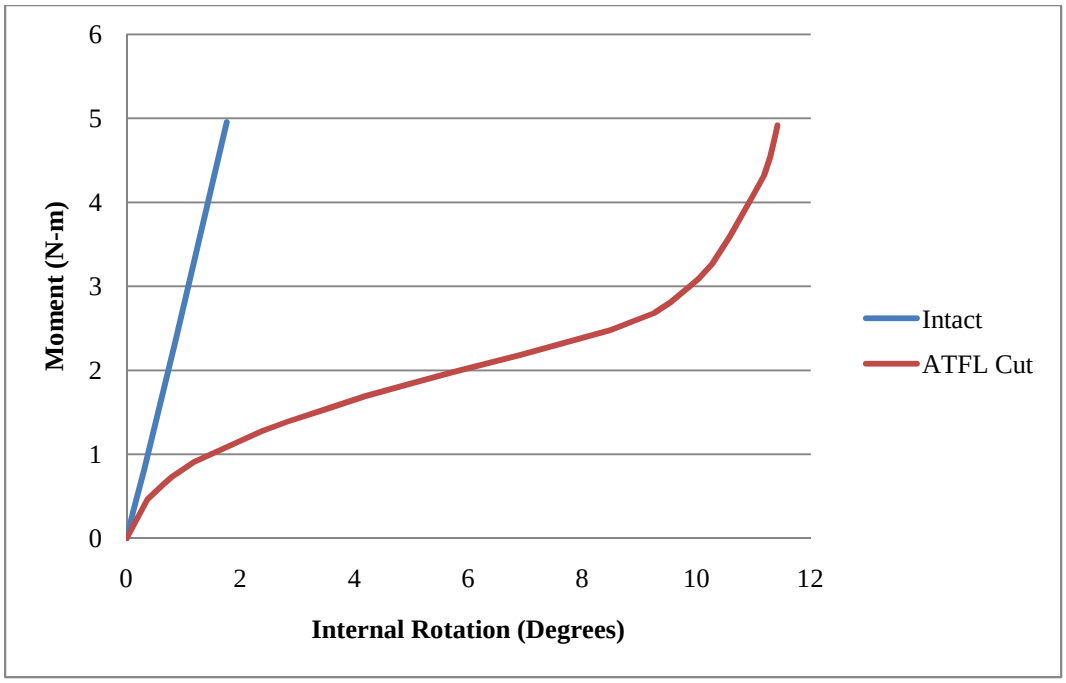

Figure 8 FEA Model Moment vs. Internal Rotation

The figure shows the change in Internal Rotation vs. Moment for the finite element model. The intact model shows a linear curve for load vs. displacement this is because of the linear elastic model that was used to model the ligament material properties. The ATFL cut model shows a non-linear curve, but once the DPTTL starts to carry tension forces the curve becomes increasingly linear and approaches the slope of the intact model.

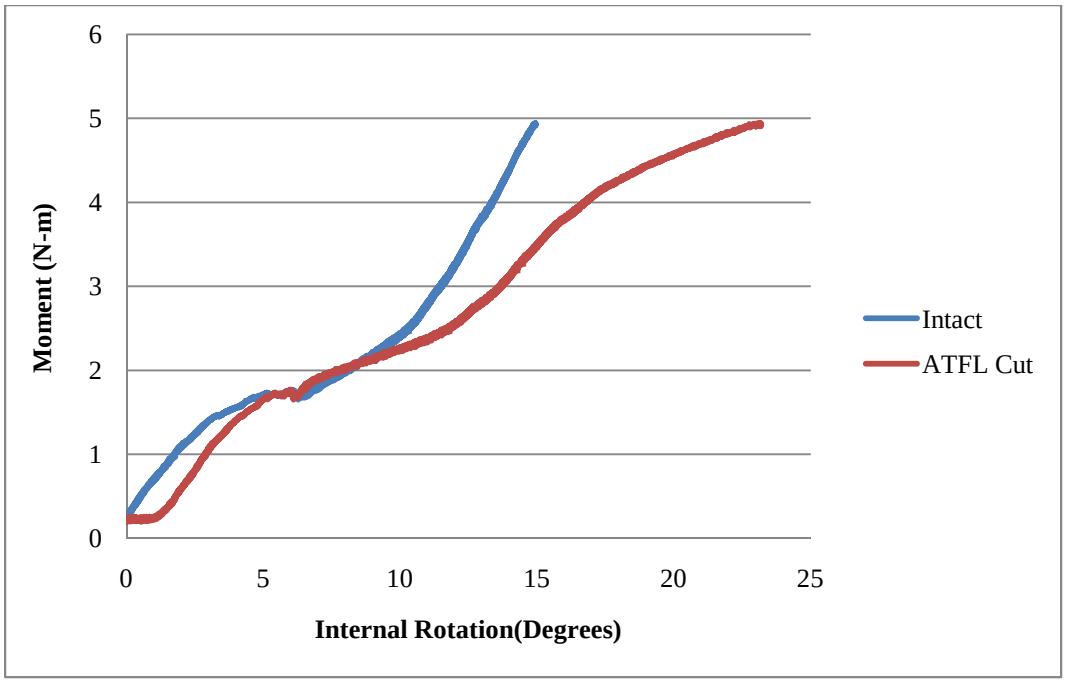

Figure 9 In Vitro Testing Moment vs. Internal Rotation

The figure shows the in Internal Rotation vs. Moment for the in vitro testing conducted on the MTS 858 Mini Bionix. While the magnitude of the maximum internal rotation varies greatly from the FEA model the relative change in magnitude from the intact to ATFL cut states is 86% of the change predicted by the FEA model.

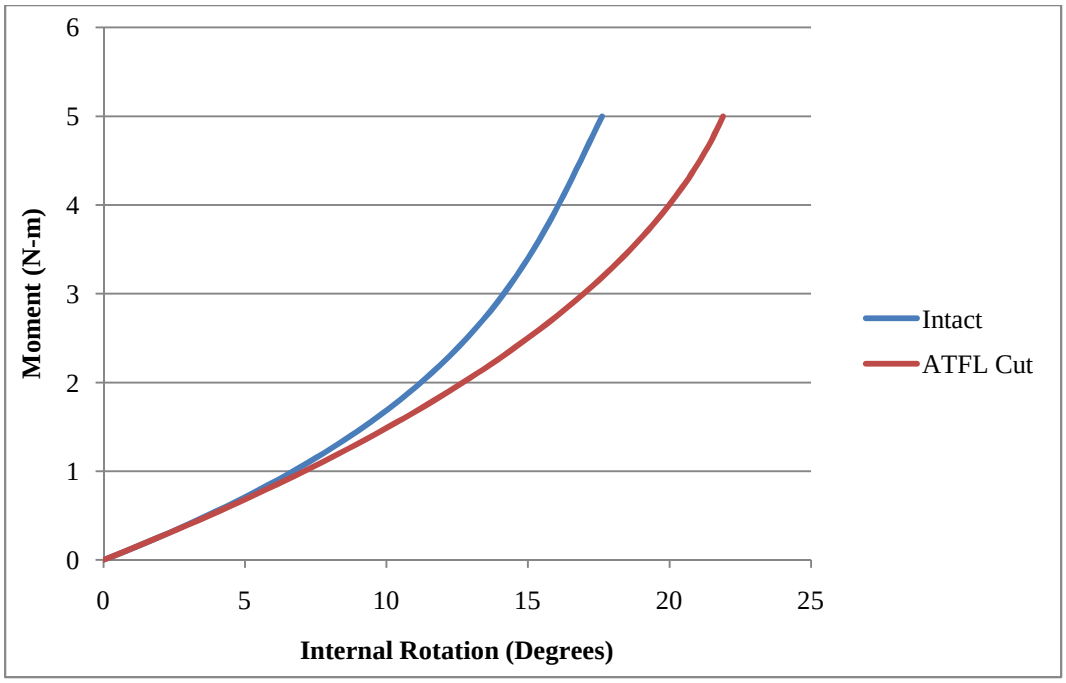

Figure 10 Arthrometer Moment vs. Internal Rotation

The figure shows the in Internal Rotation vs. Moment for the in vitro testing of the arthrometer. The arthrometer data shown has been curve fitted and standardized to facilitate comparison. The overall change in magnitude between the intact and ATFL cut state are 44% of the predicted change from the FEA model. The is due to the fact that the arthrometer uses a different set of boundary conditions and allows for movement of the subtalar and the transverse tarsal joints, as well as anterior translation during internal rotation in the intact state. (Wilkerson, Doty, et al. 2010 (in press))

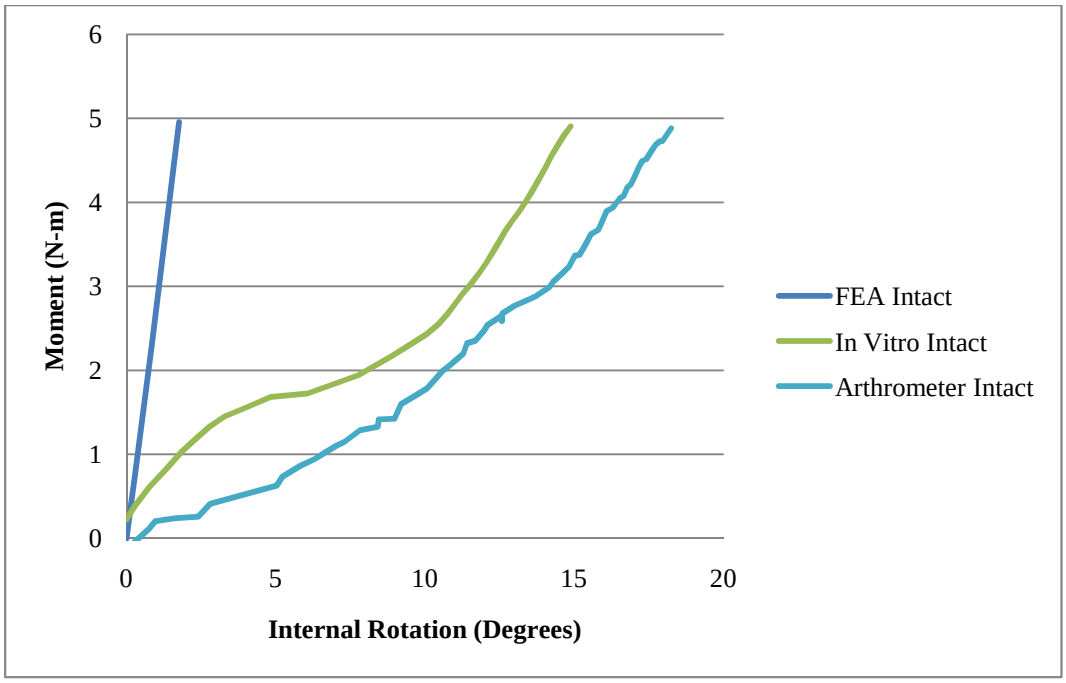

Figure 11 Comparisons of Intact State Data

The figure shows a comparison of all three testing methods in the intact state. The FEA model is linear and stiffer than the other two graphs due to the linear elastic model used for the ligament material properties. The arthrometer data is greater than in vitro results because it allows for movement of the subtalar and the transverse tarsal joints, as well as anterior translation during internal rotation.

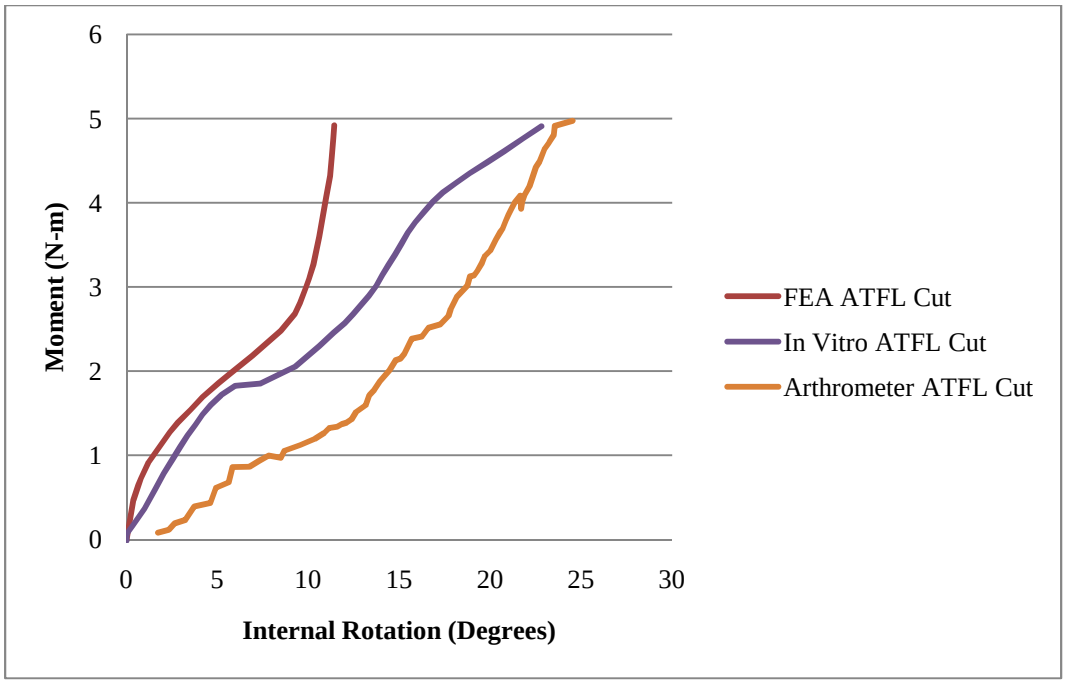

Figure 12 Comparisons of ATFL Cut State Data

The figure shows a comparison of all three testing methods in the ATFL cut state. Initially the in vitro test data follows the FEA model then shifting closer to the results of the arthrometer. This is due to the FEA model overestimating the stiffness of the ligaments by only considering the linear portion of the stress strain curve, while the arthrometer allows for movement of the subtalar and the transverse tarsal joints, as well as anterior translation during internal rotation.

Table 6 FEA Model Ligament Forces at Max Internal Rotation

Force (N)	CFL	ATFL	PTFL	DPTTL	DATTL	TCL	TNL
Intact	0	179.37	0	0	0	0	0
ATFL Cut	7.28	0	0	155.75	0	0	0

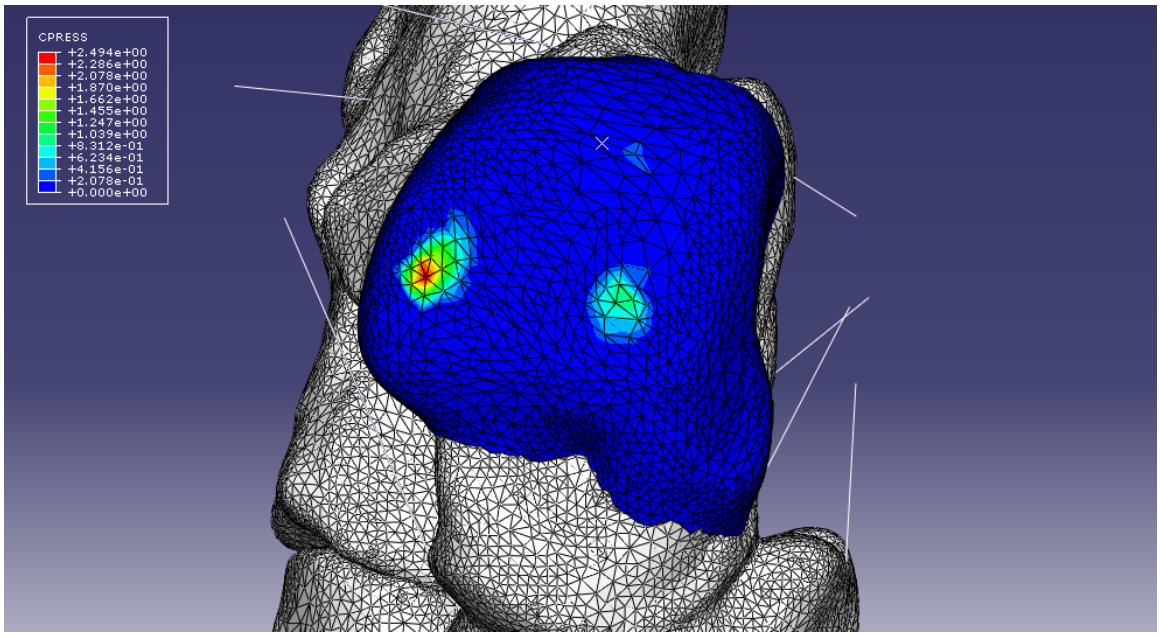

Figure 13 Intact State 0 N-m Moment Contact Pressure

The figure shows the intact state model's contact pressure at 0 N-m of moment applied. Loading is spread over two points on the medial and lateral sides of the talar dome, with the highest concentration on the lateral side.

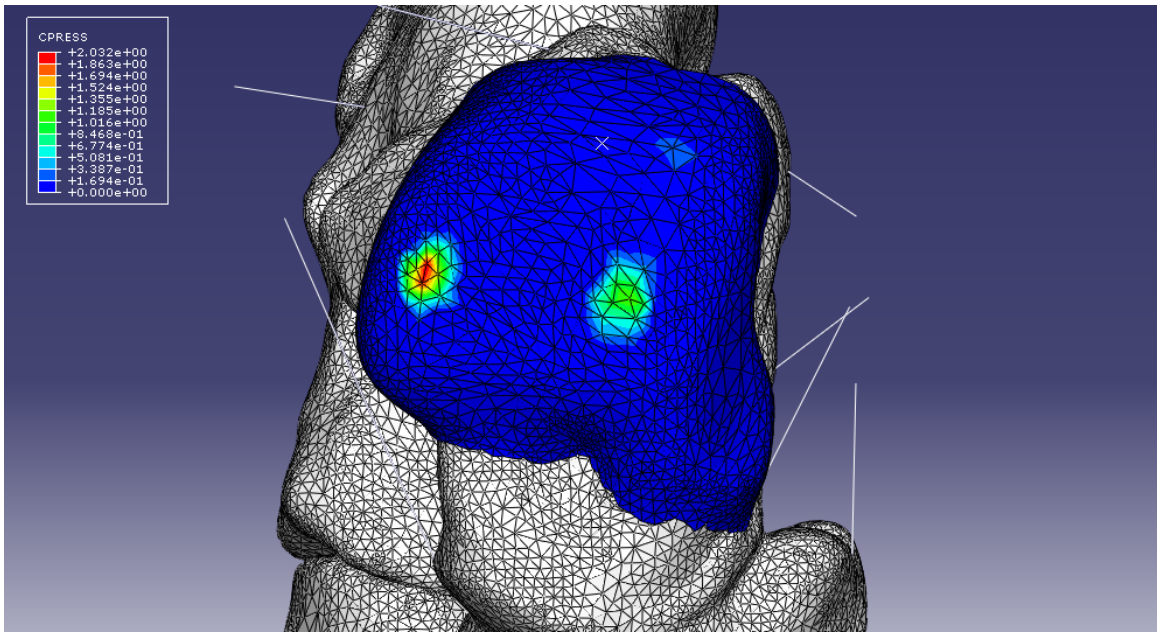

Figure 14 Intact State 5 N-m Moment Contact Pressure

The figure shows the intact state model's contact pressure at 5 N-m of moment applied. Loading is spread over two points on the medial and lateral sides of the talar dome, with the highest concentration on the lateral side. This is a similar distribution to the 0 N-m moment contact pressure image shown in Figure 12.

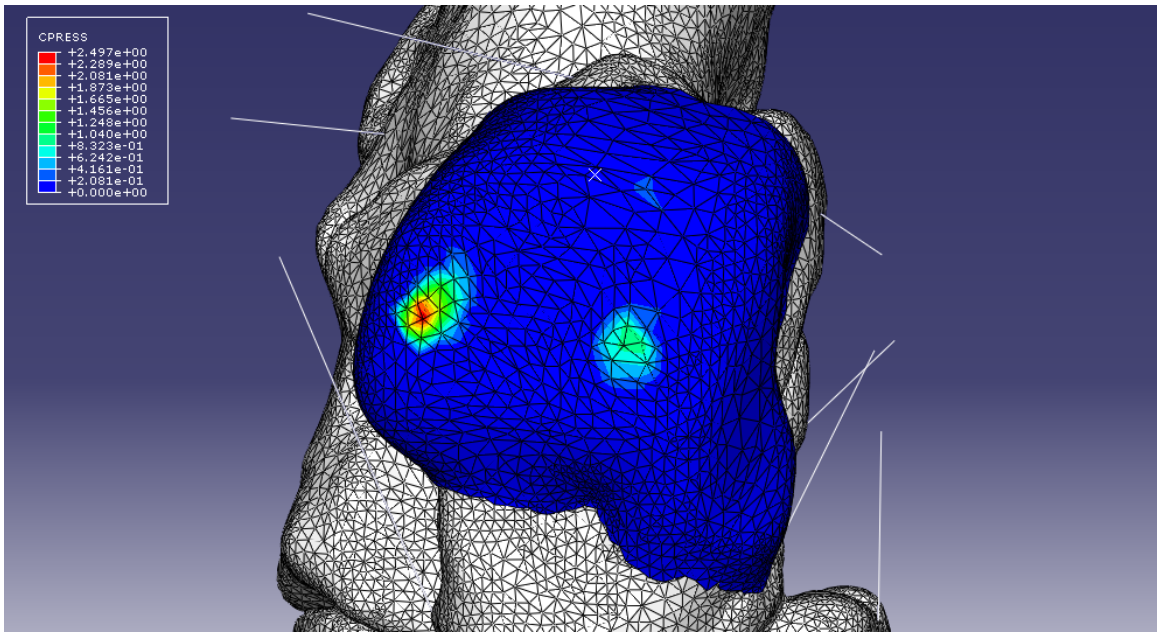

Figure 15 ATFL Cut State 0 N-m Moment Contact Pressure

The figure shows the ATFL cut state model's contact pressure at 0 N-m of moment applied. Loading is spread over two points on the medial and lateral sides of the talar dome, with the highest concentration on the lateral side.

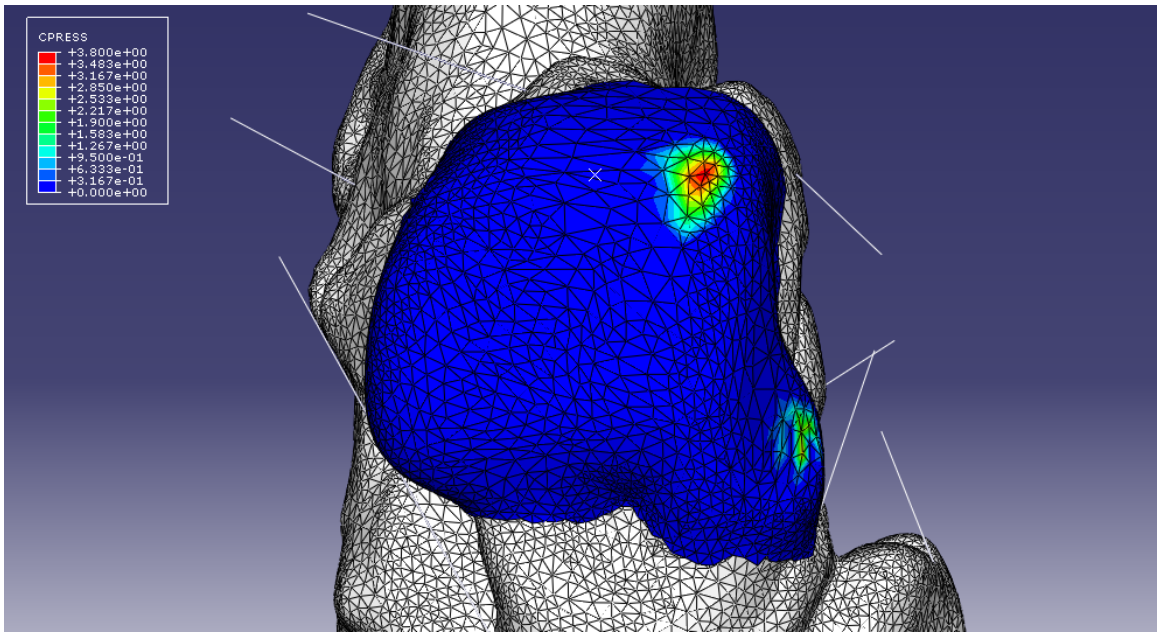

Figure 16 ATFL Cut State 5 N-m Moment Contact Pressure

The figure shows the ATFL cut state model's contact pressure at 5 N-m of moment applied. Contact has shifted to the posterior medial side of the talar dome and to anterior portion of the facet for the tibia malleolus. Both locations have been shown to be locations of articular cartilage lesions in patients with lateral ankle instability. (Taga, et al. 1993, Hintermann, Boss and Schafer 2002, Valderrabano, et al. 2006, van Dijk, Bossuyt and Marti 1996)

Chapter 5 Conclusions

The results show a correlation in the change in magnitude from intact to ATFL cut states in the FEA model to the in vitro test on the MTS of 86% of the predicted value. The arthrometer data shows a change that is 44% of the predicted amount. The arthrometer has a greater degree of freedom from less restrictive boundary conditions coupled with free movement of the subtalar and transverse tarsal joints because of this it can internally rotate to a greater degree with the ATFL intact. The FEA model results show a linear behavior that is a result of linear elastic material ligament model used in the model. The ligament's true material behavior is a non-linear viscoelastic material. (Mow and Huiskes 2005) In the contact analysis results the model predicts a medial shift in contact pressures under internal rotation without the ATFL which has been shown to be a potential location for lesions in ankles with lateral instability. (van Dijk, Bossuyt and Marti 1996, Hintermann, Boss and Schafer 2002, Taga, et al. 1993, Valderrabano, et al. 2006, Okuda, et al. 2005) The model also predicts that the DPTTL and not the CFL carries a majority of the resistant forces in the ligaments in internal rotation when the ATFL has been compromised. This of interest because there has been some debate on rather the CFL or the DPTTL is injured by internal rotation after the disruption of the ATFL, and the model results do not show that the CFL sees any significant stress. (Stormont, et al. 1985, Rasmussen and Tovborg-Jensen, Anterolateral Rotational Instability in the Ankle Joint 1981) In future models it would be necessary to model the surrounding soft tissue such as the joint capsule, muscles, and skin to allow for more freedom of movement without creating an under-constrained ridged body. Several other studies have done this taking into account the hyper-elastic properties of the surrounding soft tissue. (Cheung and Zhang 2006) Ligaments could also me modeled as viscoelastic and non-linear to create a more accurate look at the behavior of the ankle joint. Further areas of research could also look at the effects of various control devices such as boots or taping to prevent excessive internal rotation in an unstable ankle. (Hintermann and Valderrabano 2001, Wilkerson, et al. 2005, Omori, et al. 2004) This type of modeling would require interaction between the outer layer of soft tissue and whatever stabilization device was being examined.

List of References

List of References

3D Slicer home page. 2010. www.slicer.org.

Abaqus, Version 6.7-3. *Abaqus Analysis User's Manual Version 6.7-3.* Dassault Systemes, 2007.

American Academy of Orthopaedic Surgeons. *Joint Motion. Method of Measuring and Recording.* Chicago: AAOS, 1965.

Anderson, Donald D, et al. "Intra-articular Contact Stress Distribution at the Ankle throughout Stance Phase - Patient-Specific Finite Element Analysis as a Metric of Degeneration Propensity." *Biomech Model Mechanobiol* 5 (2006): 82-89.

Attarian, David E, Hugh J McCrackin, Dennis P DeVito, James H McElhaney, and William E Garrett. "Biomechanical Characteristics of Human Ankle Ligaments." *Foot & Ankle* 6, no. 2 (1985): 54-58.

Birmingham, Trevor B, Bret M Chesworth, Heather D Hartsell, Anne L Stevenson, Garry L Lapenskie, and Anthony A Vanderwoort. "Peak Passive Resistive Torque at Maximum Inversion Range of Motion in Subjects With Recurrent Ankle Inversion Sprains." *Journal of Orthopaedic & Sports Physical Therapy* 25, no. 5 (1997): 342-348.

Cheung, Jason Tak-Man, and Ming Zhang. "Finite Element Modeling of the Human Foot and Footwear." *ABAQUS Users' Conference.* Cambridge, Massachusetts: Simulia, 2006. 145-159.

Colville, Mark R, Richard A Marder, John J Boyle, and Bertram Zarins. "Strain measurement in lateral ankle ligaments." *The American Journal of Sports Medicine* 18, no. 2 (1990): 196-200.

Conlin, F Dixson, Paul G Johnson, and John E Sinning. "The Etiology and Repair of Rotary Ankle Instability." *Foot & Ankle* 10, no. 3 (1989): 152-155.

Dias, Luciano S. "The Lateral Ankle Sprain: An Experimental Study." *The Journal of Trauma* 19, no. 4 (1979): 266-269.

El-Khoury, Georges Y, Kyle J Alliman, Hannah J Lundberg, Melvin J Rudert, Thomas D Brown, and Charles L Saltzman. "Cartilage Thickness in Cadaveric Ankles: Measurement with Double-Contrast Multi-Detector Row CT Arthrography versus MR Imaging." *Radiology* 233 (2004): 768-773.

Gering, D, et al. "An Integrated Visualization System for Surgical Planning and Guidance using Image Fusion and Interventional Imaging." *Int Conf Med Image Comput Comput Assist Interv.* 1999. 809-819.

Hintermann, B, and V Valderrabano. "The effectiveness of rotational stabilization in the conservative treatment of severe ankle sprains: a long-term investigation." *Foot and Ankle Surgery* 7 (2001): 235-239.

Hintermann, Beat, Andreas Boss, and Dirk Schafer. "Arthroscopic Findings in Patients with Chronic Ankle Instability." *The American Journal of Sports Medicine* 30, no. 3 (2002): 402-408.

Iaquinto, Joseph M, and Jennifer S Wayne. "Correlation Between 3D Computational Prediction of Mechanical Function and Simulated Physical Weightbearing in the Cadaveic Lower Leg." *Summer Bioengineering Conference.* Marco Island, Flordia: ASME, 2008. 1-2.

Johnson, Eric E, and Keith L Markolf. "The Contribution of the Anterior Talofibular Ligament to Ankle Laxity." *The Journal of Bone and Joint Surgery* 65-A, no. 1 (1983): 81-88.

Mann, Roger A, and Andrew Haskell. "Biomechanics of the Foot and Ankle." In *Surgery of the Foot and Ankle*, by Michael J Coughlin, Roger A Mann and Charles L Saltzman, 3-180. Philiadelphia: Mosby, 2007.

Mansour, Joseph M. "Biomechanics of Cartilage." Chap. 5 in *Kinesiology: The Mechanics and Pathomechanics of Human Movement*, by Carol A. Oatis, 66-79. Philadelphia: Lippincott Williams and Wilkins, 2004.

McCullough, C J, and P D Burge. "Rotatory Stability of the Load-Bearing Ankle." *Journal of Bone and Joint Surgery British* 62-B, no. 4 (1980): 460-464.

Mkandawire, Chimba, William R Ledoux, Bruce J Sangeorzan, and Randal P Ching. "Foot and ankle ligament morphometry." *Journal of Rehabilitation Research & Development* 42, no. 6 (2005): 809-819.

Mow, Van C, and Rik Huiskes. *Basic Orthopaedic Biomechanics and Mechano-Biology.* 3rd. Philadelphia: Lippincott Williams & Wilkins, 2005.

Netter, Frank H. *Atlas of Human Anatomy.* Teterboro, NJ: Icon Learning Systems, 2003.

Okuda, Ryuzo, Mitsuo Kinoshita, Junichi Morikawa, Toshito Yasuda, and Muneaki Abe. "Arthroscopic Findings in Chronic Lateral Ankle Instability: Do Focal Chondral Lesions Influence the Results of Ligament reconstruction?" *The American Journal of Sports Medicine* 33, no. 1 (2005): 35-41.

Omori, Go, Kensaku Kawakami, Makoto Sakamoto, Toshiaki Hara, and Yoshio Koga. "The effect of an ankle brace on the 3-dimensional kinematics and tibio-talar contact condition for lateral ankle sprains." *Knee Surg Sports Traumatol Arthrosc* 12 (2004): 457-462.

Parlasca, Robert, Hiromu Shoji, and Robert D D'Ambrosia. "Effects of Ligamentous Injury on Ankle and Subtalar joints: A Kinematic Study." *Clinical Orthopaedics and Related Research* 140 (1979): 266-272.

Pieper, S, B Lorensen, W Schroeder, and R Kikinis. "The NA-MIC Kit: ITK, VTK, Pipelines, Grids and 3D Slicer as an Open Platform for the Medical Image Computing Community." *Proceedings of the 3rd IEEE International Symposium on Biomedical Imaging: From Nano to Macro.* 2006. 698-701.

Pieper, S, M Halle, and R Kikinis. "3D SLICER." *Proceedings of the 1st IEEE International Symposium on Biomedical Imaging: From Nano to Macro.* 2004. 632-635.

Rasmussen, Ove, and Claus Kromann-Andersen. "Experimental Ankle Injuries." *Acta orthop. scand.* 54 (1983): 356-362.

Rasmussen, Ove, and Ib Tovborg-Jensen. "Anterolateral Rotational Instability in the Ankle Joint." *Acta orthop. scand.* 52 (1981): 99-102.

Renstrom, P, et al. "Strain in the Lateral Ligaments of the Ankle." *Foot & Ankle* 9, no. 2 (1988): 59-63.

Shepherd, D E T, and B B Seedhorn. "Thickness of human articular cartilage in joints of the lower limb." *Am Rheum Dis* 58 (1999): 27-34.

Siegler, Sorin, John Brock, and Carson D Schneck. "The Mechanical Characteristics of the Collateral Ligaments of the Human Ankle Joint." *Foot & Ankle* 8, no. 5 (1988): 234-242.

St. Pierre, Rick K, Jeffrey Rosen, Thomas E Whitesides, Myron Szczukowski, Lamar L Fleming, and William C Hutton. "The Tensile Strength of the Anterior Talofibular Ligament." *Foot & Ankle* 4, no. 2 (1983): 83-85.

Stormont, Daniel M, Bernard F Morrey, Kai-Nan An, and Joseph R Cass. "Stability of the loaded ankle: Relation between articular restraint and primary and secondary static restraints." *The American Journal of Sports Medicine* 13, no. 5 (1985): 295-300.

Taga, Ichiro, Konsei Shino, Masahiro Inoue, Ken Nakata, and Akira Maeda. "Articular cartilage lesions in ankles with lateral ligament injury: An arthroscopic study." *The American Journal of Sports Medicine* 21, no. 1 (1993): 120-127.

Teramoto, Atsushi, Hideji Kura, Eiichi Uchiyama, Daisuke Suzuki, and Toshihiko Yamashita. "Three-Dimensional Analysis of Ankle Instability After Tibiofibular Syndesmosis Injuries." *Am J Sports Med* 36 (2008): 348-352.

Valderrabano, Victor, Beat Bintermann, Monika Horisberger, and Tak Shing Fung. "Ligamentous Posttraumatic Ankle Osteoarthritis." *The American Journal of Sports Medicine* 34, no. 4 (2006): 612-620.

van Dijk, C N, P M Bossuyt, and R K Marti. "Medial Ankle Pain After Lateral Ligament Rupture." *Journal of Bone and Joint Surgery British* 78-B (1996): 562-567.

Wilkerson, G B, and R G Alvarez. "Rotary ankle instability: Pathomechanics and consequences of inadequate treatment." *Athl Ther Today*, 2010 (in press).

Wilkerson, G B, J Doty, J M Hollis, and L R Gurchiek. "Rotary ankle instability: Effects of Sequential Sectioning of Cadaver Ankle Ligaments and Restraint Provided by Ankle Taping." *Athl Ther Today*, 2010 (in press).

Wilkerson, Gary B, John E Kovaleski, Mark Meyer, and Christopher Stawiz. "Effects of the Subtalar Sling Ankle Taping Technique on Combined Talocrural-Subtalar Joint Motions." *Foot & Ankle International* 26, no. 3 (2005): 239-246.

Xenos, J S, W J Hopkinson, M E Mulligan, E J Olson, and N A Popovic. "The tibiofibular syndesmosis. Evaluation of the ligamentous structures, methods of fixation, and radiographic assessment." *J Bone Joint Surg Am.* 77 (1995): 847-856.

Appendix

ABAQUS Input File

```
*HEADING
Written by Bain Ervin
*RESTART,WRITE,FREQUENCY = 10,OVERLAY
*NODE
         1,  99.340984779952,  102.20434363817,  -65.2193159176
           .
           .
           .
    78591,  112.6631832246 ,  69.784731694166,  -92.13478344022
*ELEMENT,TYPE=C3D4,ELSET=Fibula
     5663,     2834,      223,     3289,      214
           .
           .
           .
    19451,      284,      289,     3195,      324
*ELEMENT,TYPE=C3D4,ELSET=Tibia
    46248,     4338,     4253,    17752,     4438
           .
           .
           .
    72934,    19171,     5452,     5379,     5318
*ELEMENT,TYPE=C3D4,ELSET=Calcaneus
    72935,    21032,     9432,     9486,     9462
           .
           .
           .
   120215,    20536,    12730,    20244,    12803
*ELEMENT,TYPE=C3D4,ELSET=Talus and Fore Foot
   180994,    29966,    55262,    30065,    59932
           .
           .
           .
   357033,    34933,    34488,    34725,    34806
*ELEMENT,TYPE=C3D6,ELSET=Talus Cart
   357034,    27648,    27822,    27928,    69679,    69680,    69681
           .
           .
           .
   366864,    74750,    74735,    74753,    74751,    74736,    74754
*ELEMENT,TYPE=C3D6,ELSET=Tibia Cart
   366865,     5041,     5040,     5038,    74797,    74798,    74799
           .
           .
           .
   373941,    78530,    78527,    78590,    78531,    78528,    78591
*ELEMENT, TYPE=T3D2, ELSET=CFL
   373942,    13062,       91
*ELEMENT, TYPE=T3D2, ELSET=ATFL
```

```
   373943,     27846,      1115
*ELEMENT, TYPE=T3D2, ELSET=PTFL
   373944,      885,     26108
*ELEMENT, TYPE=T3D2, ELSET=DPTTL
   373945,     5084,     26064
*ELEMENT, TYPE=T3D2, ELSET=DATTL
   373946,     5454,     27652
*ELEMENT, TYPE=T3D2, ELSET=TCL
   373947,     5486,     15163
*ELEMENT, TYPE=T3D2, ELSET=TNL
   373948,     5618,     24472
*NSET, NSET=Prox
     2390,     2393,     2394,     2395,     2397,     2398,     2404,     2407,
             .
             .
             .
    19484,     19493,     19494,     19496,     19502
*NSET, NSET=Dist
     8929,     8930,     8931,     8932,     8933,     8934,     8935,     8936,
             .
             .
             .
    69479,     69596,     69638
*ELSET, ELSET=Tal-Cont
   357036,    357039,    357042,    357045,    357048,    357051,    357054,    357057,
             .
             .
             .
   366852,    366855,    366858,    366861,    366864
*ELSET, ELSET=Tib-Cont
   366867,    366870,    366873,    366876,    366879,    366882,    366885,    366888,
             .
             .
             .
   373923,    373926,    373929,    373932,    373935,    373938,    373941
*ELSET, ELSET=Fib-Cont
     5664,     5665,     5667,     5670,     5676,     5678,     5680,     5688,
             .
             .
             .
    19427,     19429,     19434,     19436,     19444,     19446,     19447,     19451
*NSET, NSET=Prox-1
     4465,
*NSET, NSET=Dist-1
    29869,
*****
*****Materials Defined**************************************
*****
*MATERIAL, NAME=Bone
*ELASTIC
16000.0,0.3
```

```
*DENSITY
1.5E-9
*MATERIAL, NAME=Cartilage
*ELASTIC
10.0,0.3
*DENSITY
1.0E-9
*MATERIAL, Name=Ligament
*ELASTIC
158.0,0.3
*NO COMPRESSION
*DENSITY
1.0E-9
**
*SOLID SECTION, ELSET=Tibia, MATERIAL=Bone
*SOLID SECTION, ELSET=Calcaneus, MATERIAL=Bone
*SOLID SECTION, ELSET=Talus and Fore Foot, MATERIAL=Bone
*SOLID SECTION, ELSET=Fibula, MATERIAL=Bone
*SOLID SECTION, ELSET=Talus Cart, MATERIAL=Cartilage
*SOLID SECTION, ELSET=Tibia Cart, MATERIAL=Cartilage
*SOLID SECTION, ELSET=CFL, MATERIAL=Ligament
21.36
*SOLID SECTION, ELSET=ATFL, MATERIAL=Ligament
62.85
*SOLID SECTION, ELSET=PTFL, MATERIAL=Ligament
46.43
*SOLID SECTION, ELSET=DPTTL, MATERIAL=Ligament
78.43
*SOLID SECTION, ELSET=DATTL, MATERIAL=Ligament
43.49
*SOLID SECTION, ELSET=TCL, MATERIAL=Ligament
43.20
*SOLID SECTION, ELSET=TNL, MATERIAL=Ligament
60
*****
*****CREATING SURFACES FROM ELEMENTS FOR CONTACT**********
*****
*SURFACE, NAME = Tib-Cont, TYPE = ELEMENT, TRIM = YES
Tib-Cont,
*SURFACE, NAME = Tal-Cont, TYPE = ELEMENT, TRIM = YES
Tal-Cont,
*SURFACE, NAME = Fib-Cont, TYPE = ELEMENT, TRIM = YES
Fib-Cont,
*****
*CONTACT PAIR, INTERACTION=cont1
Tib-Cont,Tal-Cont
Fib-Cont,Tal-Cont
Tal-Cont,Tib-Cont
**
*SURFACE INTERACTION, NAME = cont1
*SURFACE BEHAVIOR, PRESSURE-OVERCLOSURE = EXPONENTIAL
```

```
.0001,.01
**
*FRICTION, TAUMAX = 0.000000001
0.001
*****
*****TYING NODE SETS TO SINGLE NODE***************
*****
*RIGID BODY, TIE NSET=Prox, REF NODE=Prox-1
*RIGID BODY, TIE NSET=Dist, REF NODE=Dist-1
*****
*BOUNDARY
Prox-1,1,6,0
**
********************************************************************************
**HMNAME LOADSTEP         1 pre axial position
*STEP, INC =         1000, NAME = Pre Axial Position, NLGEOM = YES
*STATIC
0.01     ,1.0      ,1.0000E-07,1.0
**
*BOUNDARY, OP=NEW
Dist-1,1,1,0
Dist-1,2,2,-1.0
Dist-1,3,6,0
Prox-1,1,6,0
**
*NODE PRINT, FREQUENCY = 500
u
rf
coord
*OUTPUT, FIELD, FREQUENCY =5
*NODE OUTPUT
U, RF
*ELEMENT OUTPUT
S, E
*CONTACT OUTPUT
cstress
*END STEP
********************************************************************************
**HMNAME LOADSTEP         2 axial load 100N (Single Leg Stance 150lbf)
*STEP, INC = 1000, NAME = Axial Load 100N, NLGEOM = YES, AMPLITUDE=RAMP
*DYNAMIC, HAFTOL =20000
0.01     ,5.0      ,1.0000E-07,5.0
**
*CONTACT CONTROLS, STABILIZE
*CONTACT CONTROLS, AUTOMATIC TOLERANCES
*CONTROLS, ANALYSIS = DISCONTINUOUS
**
*BOUNDARY, OP=NEW
Dist-1,4,4,0
Prox-1,1,6,0
**
```

```
*CLOAD, OP=NEW
Dist-1,2,-100
**
*NODE PRINT, FREQUENCY = 500
u
rf
coord
*OUTPUT, FIELD, FREQUENCY =5
*NODE OUTPUT
U, RF
*ELEMENT OUTPUT
S, E
*CONTACT OUTPUT
cstress
*END STEP
******************************************************************************
**HMNAME LOADSTEP         3 Rotational Displacement 1
*STEP, INC = 1000, NAME = Rot Disp 1, NLGEOM = YES
*STATIC
0.01     ,1.0      ,1.0000E-07,1.0
**
*CONTACT CONTROLS, RESET
**
*CHANGE FRICTION, INTERACTION = cont1
*FRICTION, TAUMAX = 0.0
0.0
**
*BOUNDARY, FIXED
Dist-1,3,4
**
*CLOAD, OP=MOD
Dist-1,5,-5000
**
*NODE PRINT, FREQUENCY = 500
u
rf
coord
*OUTPUT, FIELD, FREQUENCY =5
*NODE OUTPUT
U, RF
*ELEMENT OUTPUT
S, E
*CONTACT OUTPUT
cstress
*END STEP
******************************************************************************
**HMNAME LOADSTEP         4 Rotational Displacement 2
*STEP, INC = 1000, NAME = Rot Disp 2, NLGEOM = YES
*STATIC
0.01     ,1.0      ,1.0000E-07,1.0
**
```

```
*CLOAD, OP=MOD
Dist-1,5,0
**
*NODE PRINT, FREQUENCY = 500
u
rf
coord
*OUTPUT, FIELD, FREQUENCY =5
*NODE OUTPUT
U, RF
*ELEMENT OUTPUT
S, E
*CONTACT OUTPUT
cstress
*END STEP
**********************************************************************************
**HMNAME LOADSTEP         5 Remove ATFL
*STEP, INC = 1000, NAME = Remove ATFL, NLGEOM = YES
*STATIC
0.25     ,1.0      ,1.0000E-07,1.0
**
*CONTACT CONTROLS, RESET
**
*BOUNDARY, FIXED
Dist-1,1,1
Dist-1,3,6
**
*MODEL CHANGE, Remove
ATFL,
**
*NODE PRINT, FREQUENCY = 500
u
rf
coord
*OUTPUT, FIELD, FREQUENCY =5
*NODE OUTPUT
U, RF
*ELEMENT OUTPUT
S, E
*CONTACT OUTPUT
cstress
*END STEP
**********************************************************************************
**HMNAME LOADSTEP         6 Rotational Displacement With out ATFL 1
*STEP, INC = 1000, NAME = Rot Disp wo ATFL 1, NLGEOM = YES
*STATIC
0.01     ,1.0      ,1.0000E-07,1.0
**
*CONTACT CONTROLS, STABILIZE=0.1
*CONTACT CONTROLS, AUTOMATIC TOLERANCES
**
```

```
*CHANGE FRICTION, INTERACTION = cont1
*FRICTION, TAUMAX = 0.0
0.0
**
*BOUNDARY, OP=NEW, FIXED
Dist-1,3,4
Prox-1,1,6
**
*CLOAD, OP=MOD
Dist-1,5,-5000
**
*NODE PRINT, FREQUENCY = 500
u
rf
coord
*OUTPUT, FIELD, FREQUENCY =5
*NODE OUTPUT
U, RF
*ELEMENT OUTPUT
S, E
*CONTACT OUTPUT
cstress
*END STEP
**********************************************************************************
**HMNAME LOADSTEP         7 Rotational Displacement With out ATFL 2
*STEP, INC = 1000, NAME = Rot Disp wo ATFL 2, NLGEOM = YES
*STATIC
0.01     ,1.0       ,1.0000E-07,1.0
**
*CHANGE FRICTION, INTERACTION = cont1
*FRICTION, TAUMAX = 0.0
**
*CLOAD, OP=MOD
Dist-1,5,0
**
*NODE PRINT, FREQUENCY = 500
u
rf
coord
*OUTPUT, FIELD, FREQUENCY =5
*NODE OUTPUT
U, RF
*ELEMENT OUTPUT
S, E
*CONTACT OUTPUT
cstress
*END STEP
```

Vita

Timothy Bain Ervin was born in Cleveland, TN on January 25, 1980. He was raised in Cleveland, TN and went to grade school at George R. Stuart Elementary. Through middle and high school he was homeschooled and graduated from high school in 1998. From there, he went to the University of Tennessee, Chattanooga and received a B.S. in engineering in 2001. For the next 2 years he worked in the field of hybrid electric vehicles, and then 7 years in the field of orthopaedic biomechanical research Timothy is currently pursuing a master of science in engineering at the University of Tennessee, Chattanooga.